EarthArXiv Coversheet

Claire C. Masteller

[1] Department of Earth, Environmental, and Planetary Sciences, Washington University in St. Louis, Saint Louis, MO 63130

cmasteller@wustl.edu

This pre-print is in review at *Journal of Geophysical Research – Earth Surface* and has undergone no rounds of peer-review.

Implications of impact-energy dependent erosional efficiency on bedrock river sediment dynamics and form: 1. Reach-scale dynamics and the effective flood

Claire C. Masteller[1]

[1] Department of Earth, Environmental, and Planetary Sciences, Washington University in St. Louis, Saint Louis, MO 63130

Corresponding author: Claire C. Masteller (cmasteller@wustl.edu)

Key Points:

- Incorporation of experimentally-constrained, impact-energy-dependent rock resistance into a model for impact-driven erosion evaluates its influence on bedrock incision rates
- Impact-energy-dependent rock resistance strongly amplifies grain-size controls on bedrock detachment per unit impact
- Differences in detachment efficiency with increasing impact energy emphasizes the relative contribution of rarer, high-magnitude floods

Abstract

Bedrock river incision reflects the cumulative geomorphic work performed across a distribution of flood magnitudes and frequencies. Mechanistic models of bedrock incision by bedload impacts typically assume that bedrock resistance to erosion is constant with respect to particle impact energy. However, recent impact experiments demonstrate that rock resistance to erosion decreases systematically as impacts become more energetic. Here we incorporate experimentally constrained, impact-energy-dependent rock-resistance coefficient into the widely used saltation-abrasion model and evaluate how this modification alters predicted incision across a range of grain sizes and transport conditions. We find that allowing resistance to scale with impact energy strongly amplifies the grain-size dependence of detachment, such that coarse grains remove substantially more bedrock rock per impact. Applying the model across a full discharge distribution to evaluate long-term incision reveals that while impact-energy-dependent rock resistance does not meaningfully alter the effective floods, it shifts cumulative incision toward rarer, high-magnitude events. These results demonstrate that accounting for impact-driven differences in erosional efficiency fundamental alters how geomorphic work is distributed across floods, increasing the contribution of extremes to long-term bedrock erosion rates.

Plain Language Summary

Rivers carve into bedrock when moving sediment grains strike the channel bed. How fast a river incises depends not only on how large floods are, but also on how often they occur and how energetic sediment impacts are during those floods. Many models assume that bedrock resistance to impacts is constant, meaning low- and high-energy collisions are equally efficient at breaking rock. However, recent experiments show that more energetic impacts erode bedrock more effectively. We incorporate this behavior into a widely used bedrock erosion model to test how it alters predicted incision across different grain sizes and flow conditions. As impact energy increases, coarse grains remove substantially more rock per collision. We find that this effect that is stronger than changes to the efficiency of erosion caused by increasing flow intensity alone. When we account for the full range of floods a river experiences, from frequent small events to rare large ones, we find that energy-dependent erosion increases the relative importance of extreme floods. Our results suggest that very large floods may contribute more to long-term bedrock incision than previously expected when erosion efficiency increases with sediment impact energy.

1 Introduction

River incision into bedrock drives landscape evolution, with both channel form and incision rate reflecting the combined influence of tectonics (Kirby & Whipple, 2012; Wobus et al., 2006), climate (Ferrier, Huppert, et al., 2013; Ferrier, Perron, et al., 2013), hydrology (Forte

et al., 2022; Lague et al., 2005), and geology (Duvall et al., 2004; Mitchell & Yanites, 2021). Because bedrock incision is slow and often concentrated in rare, high-magnitude events (e.g. Hartshorn, 2002), it is difficult to measure or model directly. Most models treat incision as a detachment-limited process, neglecting downstream sediment transport (e.g. Howard & Kerby, 1983; Seidl & Dietrich, 1992; Tucker & Bras, 2000). In this framework, erosion rate scales with flow intensity – commonly expressed as unit stream power or total or excess boundary shear stress. Unit stream power is typically calculated as the product of drainage area, A (km^2), a proxy for water discharge, Q (m^3/s), and channel slope, S (m/m). This formulation, which relates downstream energy dissipation to bedrock detachment, serves as the basis of the stream power incision model (SPIM). Traditionally, SPIM assumes a constant effective discharge, neglecting the full distribution of events that drive incision (Howard, 1994; Lague et al., 2000; Tucker & Slingerland, 1994; Willgoose et al., 1991). More recent work has incorporated variable discharge, demonstrating that when erosion thresholds are significant, they strongly influence landscape evolution by controlling the fraction of the discharge distribution that contributes to bedrock incision (DiBiase & Whipple, 2011; Lague et al., 2005; Snyder et al., 2003; Tucker & Bras, 2000).

These thresholds represent the minimum flow intensity required to initiate measurable bedrock erosion. They capture the idea that not all flows can detach bedrock. Only flows exceeding this threshold, set by rock strength, sediment transport, or sediment caliber or cover, can drive incision. River sediments play a central role in this process, both shielding the bed through surface armoring and promoting erosion via abrasion (Finnegan et al., 2007, 2014; Johnson et al., 2009; Johnson & Whipple, 2010). Most stream-power-based models, however, treat rivers as effectively sediment-free, implicitly folding sediment effects into the erodibility coefficient, K ($m^{1-2m}t^{-1}$), which describes the relative efficiency with which bedrock is detached per unit stream power, which also summarize the combined influences of rock strength, uplift rate, and climate (Han et al., 2014; Hancock et al., 2011; Leonard & Whipple, 2021; Small et al., 2015). While some studies have explicitly incorporated erosion thresholds into SPIM by modifying K (e.g. DiBiase & Whipple, 2011; Scherler et al., 2017), these efforts have been agnostic to what sets these erosion thresholds. More recent work has begun to incorporate the influence of sediment transport and sediment supply on long profile evolution and bedrock channel form more directly (e.g. Gasparini et al., 2007; Yanites, 2018), but even in these treatments, the physical mechanisms driving erosion are simplified.

In contrast, mechanistic bedrock erosion models provide a more detailed representation of the processes driving bedrock erosion. The saltation-abrasion model (SAM) predicts bedrock erosion rates as a function of particle impacts, adopting an energy-based approach that explicitly links river erosion to sediment transport capacity and particle size (Sklar & Dietrich, 2004). The model integrates over many impacts using an impact rate, I_r (#/m^2/s), derived from bedload flux equations. The instantaneous erosion rate, E_i (ms^{-1}), is the product of this impact

rate, the average volume of rock eroded by an individual impact, V_{imp} (m^3), and the fraction of bedrock that is exposed to impacts, F_e (−), such that $E_i = I_r V_{imp} F_e$.

While the saltation-abrasion model explicitly models the kinetic energy delivered to the bedrock riverbed, KE_{imp} (J), by solving for particle trajectories under some imposed transport capacity, it does not directly model the bedrock detachment process. Rather, like the erodibility term, *K*, in the SPIM, the model employs a rock-resistance coefficient, k_v, which modulates the relationship between particle impact energy and the volume of material removed per unit impact, V_{imp}, such that $V_{imp} \propto KE_{imp}/k_v$. As such, larger values of k_v imply higher rock resistance, or less efficient erosion, for a given impact energy. The original SAM implementation treats the rock resistance coefficient as a constant with a value of $k_v \sim 10^6$ (Sklar & Dietrich, 2004). Importantly, this assumption of a constant k_v posits that particles impacts across all impact energies are equally efficient at detaching bedrock.

More recent work has shown that the rock resistance coefficient, k_v, can vary with lithology (Auel et al., 2017b), across field settings (Turowski et al., 2013), and with particle impact energy (Masteller et al., 2024). Specifically, Masteller et al., (2024) conducted impact experiments that identified a systematic increase in erosional efficiency, or decreasing rock resistance k_v, as impact energy increased. This observed increase in erosional efficiency ($1/k_v$,) at high impact energies is related to an observed decrease in the coefficient of restitution, or rebound, of the impacting particles. Masteller et al., (2024) hypothesized that this observed increase in erosional efficiency was indicative of enhanced energy dissipation for high energy impacts, due to increasing crack extension lengths and likelihood of crack intersection. This hypothesized enhanced crack growth ultimately results in more efficient bedrock detachment for high energy collisions, as observed by their study.

This newly identified, impact energy-dependent behavior of k_v, as observed by Masteller et al., (2024), has several implications as particle impact energies can vary in both space and time and are also closely related to flow strength. Particle impact energy, KE_{imp}, is a function of both the mass of the impacting particle and the particle's velocity as it collides with the underlying bedrock. During larger floods, peak transport capacity, defined as the dimensionless shear stress exceeding the threshold for motion, τ^*/τ_c^*, increases with increasing flow depths. As transport capacities increase, flows can mobilize larger grains and accelerate saltating particles, increasing both the mass and velocity components of impact energy (Auel et al., 2017b, 2017a; Larimer et al., 2021). Extreme floods therefore deliver disproportionately energetic collisions through the combined effects of both heavier particles impacting the riverbed as well as higher particle impact velocities overall. As such, rare, high-magnitude floods may contribute more to long-term bedrock incision than expected based on transport capacity alone, elevating their relative importance to driving bedrock incision.

Landscape-scale applications of the saltation-abrasion framework have provided insights into how variable discharge distributions may translate into long-term incision rates (Sklar &

Dietrich, 2008; Sklar & Dietrich, 2006). By upscaling the SAM, Sklar and Dietrich (2006) linked variable discharge, sediment transport, and long-term bedrock incision. This upscaled application demonstrated that moderately high-flow events, rather than the largest floods, dominate incision. Sklar and Dietrich (2006) reasoned that this relative dominance of moderate floods arises because low flows fail to mobilize sediment and very high flows are too rare to maintain sufficient bedrock exposure to drive continued abrasion. However, this previous study assumed a constant rock resistance, ultimately weighting the relative influence of all impact energies as having an equal efficiency of detaching bedrock material.

Long-term bedrock incision ultimately reflects the cumulative geomorphic work performed across the full range of discharges, or the integrated instantaneous erosion rates across flood events with a range of magnitudes and frequencies. Within this framework, the effective flood emerges as the discharge that contributes most to cumulative incision over time (Wolman & Miller, 1960). If erosional efficiency increases systematically with impact energy, then the distribution of geomorphic work across the full range of the discharge distribution may shift toward more extreme events, potentially altering the magnitude of the effective flood itself. Motivated by this possibility, we extend the SAM to incorporate impact-energy-dependent erosional efficiency and evaluate how this modification alters the partitioning of geomorphic work across the discharge distribution. Specifically, we test whether increasing erosional efficiency at high impact energies shifts the effective flood toward rarer, more extreme events, or whether long-term bedrock incision rates continue to favor moderately frequent floods. By combining experimentally constrained, energy-based scaling for rock resistance with a variable discharge framework, we quantify how particle impact energy, flow magnitude, and sediment properties together govern equilibrium bedrock incision at the reach scale.

2 Materials and Methods

2.1 Incorporation of energy-dependent rock resistance coefficient

To evaluate the relative influence of a range of particle impact velocities for bedrock incision, we incorporate an impact energy-dependent rock resistance into the upscaled saltation-abrasiom model following Sklar and Dietrich (2006). We define k_v as a function of impact kinetic energy, KE_{imp}, based on the empirical data from Masteller et al. (2024). Masteller et al. (2024) showed from repeated impact experiments that rock-resistance coefficients decrease with increasing impact energy as a greater fraction of the particle impact energy is transferred to bedrock, reducing rock resistance and driving more efficient detachment. To incorporate this observation into the SAM, we use the experimental data from Masteller et al., (2024) to specify the form of the relationship between KE_{imp} and k_v. This is necessary because it is not possible to directly constrain the fraction of energy translated to bedrock during collisions in the current framework of the SAM. Using these data, the impact-energy-dependent rock resistance coefficient can be calculated as $k_v = 839.4{KE_{imp}}^{-1.21}$.

While this empirical scaling provides a translation between impact energy and erosional resistance as described by k_v, this scaling was derived using brick as a bedrock surrogate rather than natural rock. Masteller et al., (2024) used bricks in their experiments because they are relatively homogenous, readily erodible, and consistent with previous impact experiments (Litwin Miller & Jerolmack, 2021). They also used a steel impactor. Due to the use of these materials rather than natural rock, experimentally derived rock resistance coefficients ranged from k_v= 10^2-10^4, orders of magnitude less than the commonly used value of k_v =10^6, but consistent with values of kv =10^3, for soft rocks (Auel et al., 2017b; Turowski et al., 2013). To more directly reflect the range of values reported for natural rocks, and to offer a more direct comparison to Sklar and Dietrich (2006), we rescale the impact-energy dependent rock resistance coefficient to span k_v =10^3-10^7, based on compiled values from Auel et al. (2017b).

To ensure that relative k_v values are comparable across all models explored, we apply a global rescaling procedure in which impact energies are first sampled over a representative range of grain sizes, D_{50}= 0.002-0.1 m, and flow depths, *h* = 0.06-4.5 m. The resulting impact energies span over 5 orders of magnitude and define global minimum and maximum bounds on k_v (Fig. 1a). For each model run, calculated impact energies are then mapped onto this fixed global range, ensuring that a given impact energy corresponds to the same k_v across all model experiments. We compare simulations with impact-energy-dependent, variable k_v to control runs in which rock resistance is held constant for all impacts. The constant k_v selected in this case is the geometric mean of the global range of scaled rock resistance values, k_v=1.988x10^4 (Fig. 1B).

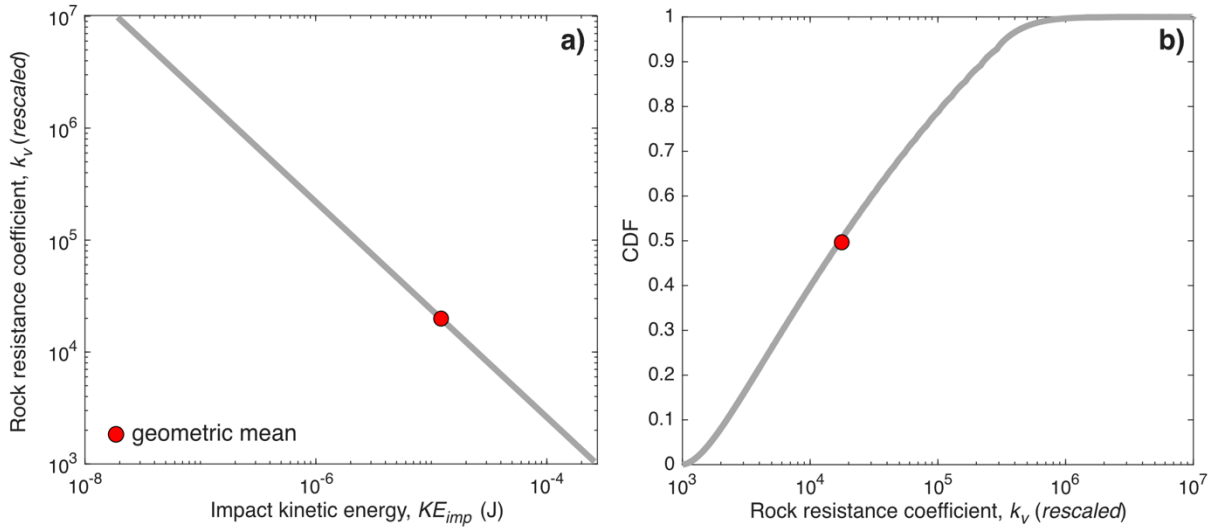

Figure 1. A) Globally scaled range of k_v values as a function of impact kinetic energy, KE_{imp}. Geometric mean $k_v$used in constant treatment of rock resistance is denoted as a red dot. B) CDF plot of globally scaled k_v values with geometric mean again denoted as a red dot.

2.2 Constant discharge case

As a first step, we isolate the influence of impact-energy-dependent k_v under a constant transport capacity, τ^*/τ_c^*, (or discharge, *Q*) condition. This simplified case allows us to examine how incorporating an impact-energy-dependent rock resistance alters the volume of rock removed per impact, V_{imp}, for a range of flood magnitudes. In the saltation-abrasion model, k_v directly scales the volume removed per bedload impact, with V_{imp} proportional to impact kinetic energy, KE_{imp}.

To evaluate how an energy-dependent k_v modifies erosion across a range of hydraulic and sediment conditions, we calculate instantaneous bedrock erosion rates, E_i, for all combinations of D_{50} = 0.002-0.1 m and τ^*/τ_c^*, = 1-10. The selected grain size range reflects moderate-sized gravel, encompassing the median grain size (D_{50}=0.06 m) reported for the South Fork Eel River, the reference site used in Sklar and Dietrich (2006, 2008). The range of selected transport capacities that encapsulates the range of incision rates modeled for the same reference site by Sklar and Dietrich (2006), where the bankfull transport capacity associated with the effective flood for the reference site is τ^*/τ_c^*=1.2. All other parameters, including reach-scale channel morphology properties and bedrock properties are consistent with Sklar and Dietrich (2006, 2008; Table S1). This constant-discharge analysis provides a baseline for understanding how impact-energy-dependent rock resistance modifies bedrock detachment rates under fixed hydraulic forcing.

2.3 Variable discharge case

We extend the constant-discharge framework to incorporate the full magnitude–frequency distribution of discharge, again guided by the South Fork Eel River reference site (Sklar and Dietrich, 2006, 2008). To isolate the role of sediment grain size in mediating the interaction between discharge variability and impact-energy-dependent erosional efficiency, all channel geometry, slope, and hydraulic scaling relationships are held constant (Table S1).

We used a 24-year record of mean daily discharge from the South Fork Eel River (USGS gage 11475500, near Branscomb), covering the same period analyzed by Sklar and Dietrich (2006). Discharges were converted to flow depth using empirical power-law relationships (Table S1). Exceedance probabilities for each flood size were then computed as one minus the cumulative distribution function, and the resulting flow-duration curve was resampled and interpolated to smooth noise and increase point density in the distribution tails where observations are sparse. Recurrence intervals for each discharge were calculated using the flow-duration curve method.

Bedrock incision was modeled using a modified saltation–abrasion framework following Sklar and Dietrich (2006), comparing a constant rock resistance coefficient with an impact-energy-dependent formulation of k_v. Median grain size was varied from D_{50} = 0.02-0.1 m, restricted compared to the constant discharge case to better reflect field-measured grain size values along the South Fork Eel River (Masteller et al., under review). Channel slope was fixed

at S = 0.0053 m/m, consistent with field measurements. For each combination of grain size and flow depth, we calculated the dimensionless transport capacity (τ^*/τ_c^*,) using standard rectangular-channel formulations. Sediment impact velocity was calculated as a function of transport capacity, grain size, and fall velocity, and the corresponding impact kinetic energy, KE_{imp}, was then computed for each flow magnitude. For the impact-energy-dependent model runs, the rock resistance coefficient, k_v, was then rescaled as a function of KE_{imp}. Bedrock incision was calculated as the product of the impract rate, I_r, the volume removed per impact, V_{imp}, and the fraction of the bedrock riverbed exposed to particle impacts, F_e, yielding modeled incision rates across the full discharge distribution for each grain size scenario.

To quantify the cumulative contribution of each flood magnitude to total bedrock incision, we multiplied the modeled instantaneous incision rates by the exceedance probability associated with each flow. This probability-weighted incision rate represents the geomorphic work performed by each discharge, integrating the relative magnitude of incision associated with each event with the frequency of occurrence for each flood size (e.g. Wolman & Miller, 1960). Framing the results in terms of geomorphic work captures both the sustained contribution of frequent flows and the relative influence of rare, high-magnitude events. From this distribution of geomorphic work across the full range of flood flows, we then identified the effective discharge, defined as the flood magnitude that contributes most to long-term erosion. We additionally constrained the relative contributions of floods within specified recurrence intervals to better isolate the influence of less frequent, higher-magnitude events.

3 Results

3.1 Constant discharge case

Calculated impact energies span many orders of magnitude, ranging from KE_{imp} = $1.89\text{x}10^{-8}$ – $2.71\text{x}10^{-4}$ J. From the saltation-abrasion model, particle impact energies increase with increasing grain size with the form $KE_{imp} \propto {D_{50}}^4$, reflecting the combined effects of increasing particle mass and impact velocity of more massive sediment. This strong nonlinear scaling between particle size and impact energy produces a heavy-tailed distribution of impact energies across the parameter space explored (Fig. S1). Because the rock-resistance coefficient scales inversely with impact energy, the corresponding k_v values decrease sharply with increasing grain size. Prior to rescaling to values representative of natural materials, k_v exhibits a strong negative dependence on grain size, with $k_v \propto {D_{50}}^{-4.84}$. This dependence arises directly from combining the mechanistic scaling between impact energy and grain size specified by the SAM with the empirically derived scaling relationship of rock resistance with impact energy from Masteller et al., (2024). Following rescaling, the exponent of the scaling relationship is reduced to $k_v \propto {D_{50}}^{-2.03}$, reflecting some compression of the dynamic range of k_v when rescaled to values representative of natural materials rather than a change in the underlying dependence of rock resistance on impact energy.

For fixed grain size, the saltation-abrasion model predicts only a weak dependence of k_v on transport capacity (see Sklar and Dietrich, 2004 for governing equations). In the SAM, impact velocity scales with excess transport capacity, such that impact energy increases as $KE_{imp} \propto (\tau^*/\tau_c^*)^{0.36}$. Incorporating this relationship into the impact-energy-dependent scaling for rock resistance implies a comparatively weak sensitivity of k_v to differences transport capacity. Consistent with this expectation, $k_v \propto (\tau^*/\tau_c^*)^{-0.44}$ for unscaled values and $k_v \propto (\tau^*/\tau_c^*)^{-0.33}$ after global rescaling. Thus, while increasing transport capacity reduces k_v, reducing rock resistance, the magnitude of this effect is modest compared to the much stronger grain-size sensitivity observed across the explored D_{50} range.

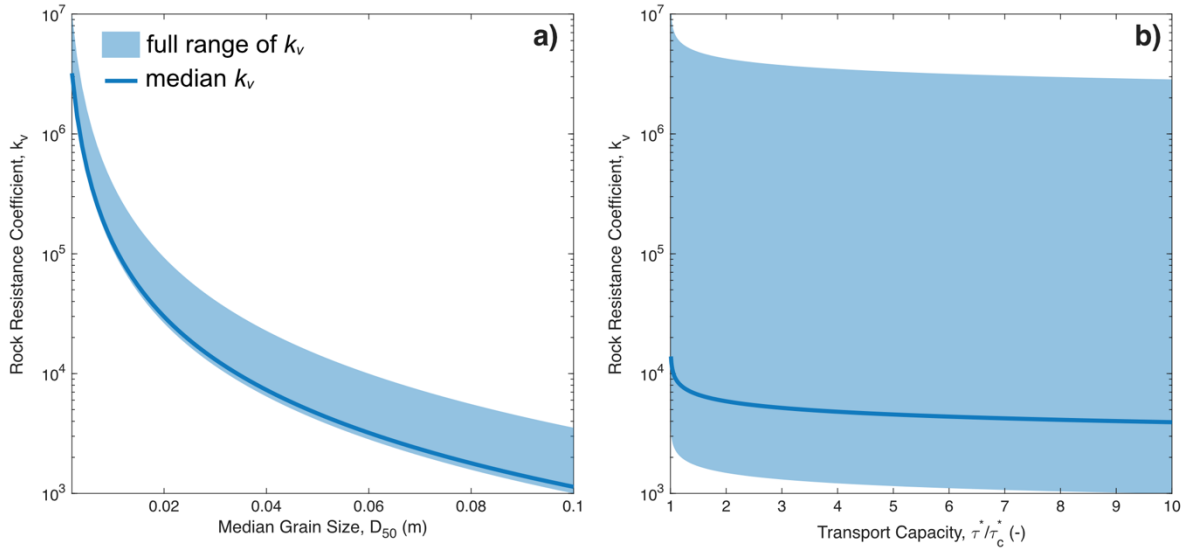

Figure 2. A) Impact-energy-dependent rock resistance coefficient, k_v, as a function of median grain size. B) Impact-energy-dependent rock resistance coefficient, k_v, as a function of transport capacity. Shading highlights range from minimum to maximum k_v, dark blue line indicates median k_v.

To place these scaling relationships in context, we evaluate how k_v varies along each axis of the model parameter space within the constant-discharge experiments (Fig. 2). When grain size is varied, the entire envelope of k_v values, spanning the full range of modeled transport capacities, decreases dramatically with increasing sediment caliber (Fig. 2A). For the finest grains considered, k_v ranges from approximately 10^6 to 10^7. In contrast, for the coarsest modeled grain sizes, k_v decreases to roughly 10^3 to 10^4. Median k_v values consistently trends toward the lower end of the envelope, indicating that typical impact conditions favor lower rock resistance and more efficient bedrock detachment. This nearly four-order-of-magnitude reduction in k_v implies that more massive grains generate greater impact energies and

297 therefore remove bedrock material far more effectively across the entire transport-capacity
298 range explored.

299 By comparison, across the full span of modeled transport capacities ($\tau^*/\tau_c^* = 1$–10), the
300 range of rock-resistance coefficients remains consistently wide (Fig. 2B). At any fixed transport
301 capacity, k_v ranges from approximately 10^3 to 10^7, reflecting the dominant role of sediment
302 grain size in setting particle impact energies, and by extension, rock resistance. Again, median
303 k_v values lie closer to the lower bound of the envelope. Although increasing transport capacity
304 slightly lowers both the minimum and maximum k_v values, the overall spread in rock resistance
305 coefficients still spans multiple orders of magnitude. Transport capacity modifies impact
306 velocity, adjusting imact kinetic energy, but grain size more strongly controls particle mass and
307 therefore exerts the primary influence on impact energy. As a result, larger grains maintain
308 substantially lower effective rock-resistance coefficients and drive more efficient bedrock
309 erosion regardless of hydraulic forcing.

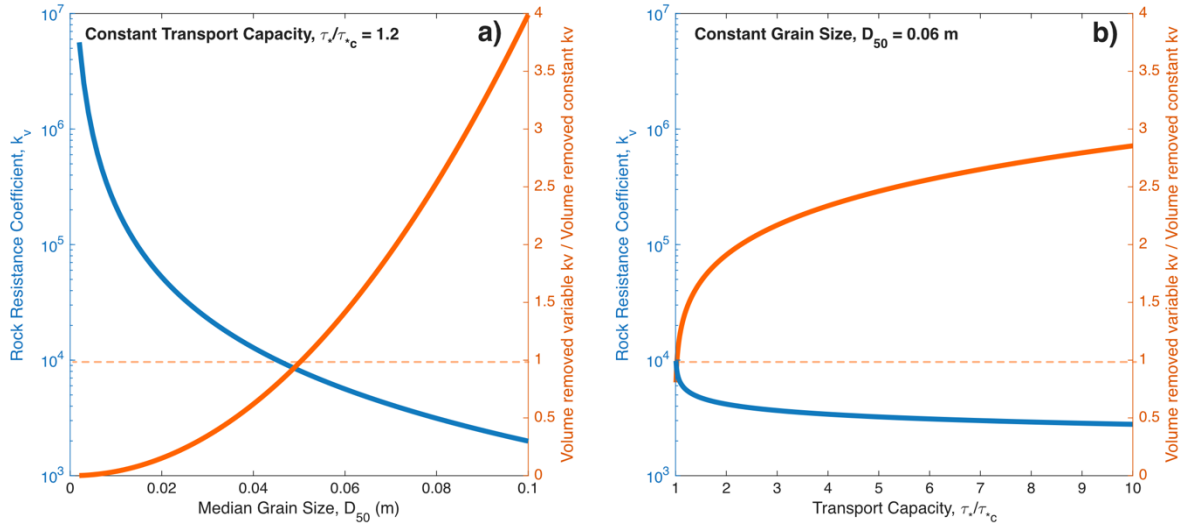

310

311 **Figure 3.** A) Rock resistance coefficient, kk_v (blue), and the ratio of volume removed per impact
312 using an impact-energy-dependent k_v relative to the constant-k_v case (red), as a function of
313 median grain size. B) Rock resistance coefficient, k_v (blue), and the ratio of volume removed
314 per impact using an impact-energy-dependent k_v relative to the constant-k_v case (red), as a
315 function of transport capacity.

316

317 These differences in the rock resistance propagate directly to the volume of bedrock
318 detached per impact, V_{imp}(Fig. 3). At constant transport capacity ($\tau^*/\tau_c^* = 1.2$), increasing grain
319 size reduces k_v by almost four orders of magnitude (Fig. 3A). This reduction produces up to a
320 four-fold increase in the volume removed per impact relative to the constant-k_v formulation.
321 Because $V_{imp} \propto D^4/k_v$, the decline in $k_v$with increasing sediment caliber compounds the
322 intrinsic scaling between grain size and impact energy within the SAM. Consequently, the

impact-energy-dependent rock resistance predicts progressively larger volumes removed per impact for coarse grains, with departures from the constant-k_v case increasing systematically beyond grain sizes of ~5 cm. For grains finer than ~ 5cm, V_{imp} for an impact-energy-dependent k_v is reduced relative to the constant-k_v case. However, this reduction largly reflects the specific value selected for the constant-k_v reference (Fig. 1), around which the global rescaling is centered. As a result, the ratio of valume remove for impact-energy-depdendent rock resistance relative to a constant k_v fall below one at low impact energies. However, the overall pattern remains that increasing grain size enhances the efficiency of bedrock detachment, with the largest grains removing the greatest volume of bedrock per impact relative to a constant rock resistance assumption.

At constant grain size ($D_{50} = 0.06$ m), increasing transport capacity reduces k_v by only about a factor of five – substantially smaller than the multiple order-of-magnitude reduction observed with increasing grain size (Fig. 3B). When coupled with the increase in impact velocity at higher τ^*/τ_c^*, this decrease in rock resistance produces up to a three-fold increase in V_{imp} relative to a constant-k_v case. Thus, although hydraulic forcing enhances detachment efficiency, its influence on the volume removed per impact remains secondary to the control exerted by sediment caliber. For a constant grain size, the largest relative increases in V_{imp} occur at transport capacities less than ~2. In this regime, small increases in excess shear stress produce relatively large increases in impact velocity and therefore impact kinetic energy. At higher transport capacities, the response of impact velocity to additional hydraulic forcing diminishes, and the relative enhancement in erosional efficiency and associated increases in V_{imp} become progressively smaller. This pattern indicates that, for a fixed grain size, moderate flows are most effective at amplifying detachment efficiency through increases in impact kinetic energy.

3.2 *Variable discharge case*

3.2.1 The effective flood and components of the saltation-abrasion model

For the variable discharge case, we first focus on the effective flood, defined as the discharge that maximizes geomorphic work when magnitude-frequency trade-offs are accounted for across the discharge distribution. We first explore the individual components of the saltation-abrasion model evaluated for the effective flood (Fig. 4).

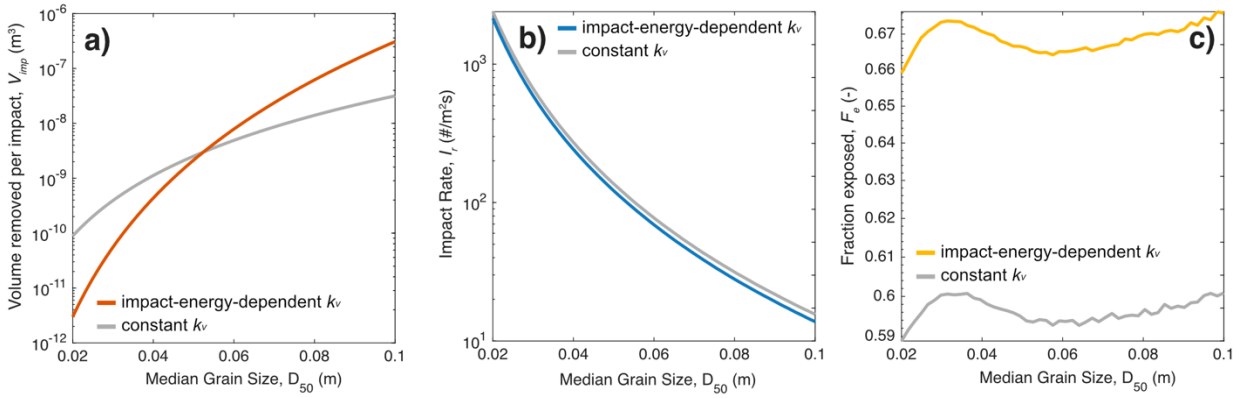

Figure 4. A) Volume removed per unit impact, V_{imp} (m^3/s), at the effective flood for impact-energy-dependent rock resistance (red) and constant rock resistance (gray), B) Impact rate, I_r (#/m2/s), at the effective flood for impact-energy-dependent rock resistance (blue) and constant rock resistance (gray), C) Fraction of bedrock exposed, F_e (-), at the effective flood for impact-energy-dependent rock resistance (yellow) and constant rock resistance (gray).

The most pronounced differences between the constant and impact-energy-dependent treatments of rock resistance emerge in the volume removed per impact, V_{imp}. Because k_v enters directly into the detachment expression, allowing rock resistance to scale with impact energy dramatically expands the range of V_{imp} at the effective flood relative to the constant-k_v case (Fig. 4a). In both formulations, V_{imp} increases with grain size, reflecting the strong scaling between particle mass and impact energy. However, this effect is amplified when the rock resistance coefficient is framed as a function of impact energy, such that k_v decreases dramatically when impacts are more energetic. Across the explored grain-size range, V_{imp} at the effective flood increases by approximately six orders of magnitude under the energy-dependent formulation of k_v, compared to only 2–3 orders of magnitude when k_v is held constant. These strong differences in V_{imp} and bedrock detachment efficiency per unit impact highlight the importance of grain size in determining the effective flood, reflecting the strong control of particle mass.

By comparison, the impact rate, I_r, and fraction of exposed bedrock, F_e, at the effective flood exhibit much smaller differences between constant and impact-energy-dependent treatments of rock resistance. Within the saltation-abrasion framework, both I_r and F_e vary as functions of excess transport capacity, $(1 - \tau^*/\tau_c^*)$, such that their values at the effective flood reflect the hydraulic transport stage that maximizes geomorphic work. Differences in I_r and F_e between constant and energy-dependent k_v formulations therefore appear to arise indirectly from changes in detachment efficiency encapsulated by V_{imp} rather than from independent modifications to transport mechanics.

Impact rate decreases systematically with increasing grain size under both constant and variable rock resistance (Fig. 4b). This decrease reflects the reduced mobility of coarse

sediment across the modeled discharge distribution. As grains become more massive and the volume removed per impact increases, fewer collisions are required to maximize geomorphic work. The decline in I_r also reflects a narrowing of the accessible transport-capacity range for coarse grains, as converting discharge to dimensionless shear stress compresses the effective transport capacity domain with increasing grain size. Incorporation of an impact-energy-dependent rock resistance produces a modest but systematic reduction in impact rate at the effective flood, which remains consistently lower, at approximately 90% of the constant-k_v values, across the modeled grain-size range.

The fraction of exposed bedrock, F_e, shows a similarly modest variation across grain sizes. Because F_e reflects the balance between sediment supply and transport capacity, it responds directly to changes in discharge and grain size. At the effective flood, F_e follows a non-monotonic pattern in both constant and energy-dependent resistance formulations (Fig. 4c). The shape of the F_e curves at the effective flood reflects how the transport state that maximizes geomorphic work evolves with grain size. In both constant and energy-dependent treatments of rock resistance, F_e increases from the fine grains to moderate grain sizes, dips slightly at these intermediate sizes, and then rises again toward the coarsest grains.

This structure emerges from shifts in the balance among imposed sediment supply (Table S1), declining impact frequency, and increasing detachment per impact. Fine, highly mobile grains generate large transport capacities and moderate exposure. As grain size increases, reduced mobility lowers transport capacity relative to supply, slightly decreasing exposure. At coarse grain sizes, however, the increase in V_{imp} shifts the effective flood toward higher transport capacities where sediment transport more consistently exceeds supply, producing an increase in F_e. The same overall pattern persists in the impact-energy-dependent k_v case, though the curve is systematically elevated relative to the constant-k_v formulation. This offset, an approximately 10-15% increase in bed exposure, reflects a shift of the effective flood toward more intense sediment transport conditions, where impact rates are reduced and bed exposure is enhanced.

Nevertheless, the magnitude of variation in both I_r and F_e remains small compared to the orders-of-magnitude divergence observed in V_{imp}. While bedrock riverbed exposure and impact rate adjust in response to the transport state, they do not appear to control the primary differences in the effective flood between constant and impact-energy-dependent treatments of rock resistance. Instead, the dominant control on bedrock incision rates and the effective flood arise from impact-energy-dependent changes in the efficiency of bedrock detachment per unit impact, V_{imp}. These component-level patterns help to clarify how the effective flood adjusts with grain size under each formulation of rock resistance. Impact rate and bed exposure respond to shifts in transport capacity, but their variations remain comparatively small. In contrast, the volume removed per unit impact varies by orders of magnitude as grain size increases, an effect that is strongly enhanced when rock resistance scales with impact energy.

The combined effect of these terms ultimately determines the instantaneous erosion rate, E_i at the effective flood.

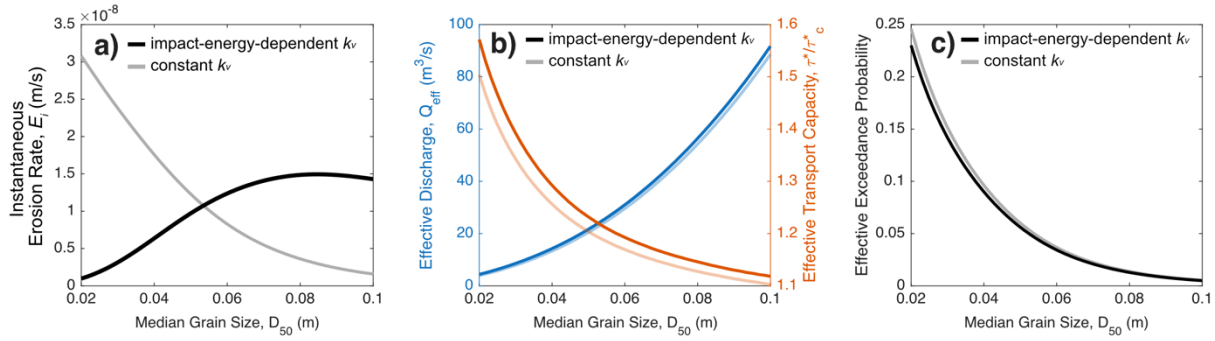

Figure 5) A) Instantaneous bedrock erosion rate, E_i (m/s), at the effective flood for impact-energy-dependent rock resistance (black) and constant rock resistance (gray), B) Effective discharge, Q_{eff} (m^3/s; left axis), and effective transport capacity, τ^*/τ_c^* (right axis) for impact-energy-dependent rock resistance (dark) and constant rock resistance (light), C) Effective flood exceedance probability for impact-energy-dependent rock resistance (black) and constant rock resistance (gray).

Instantaneous bedrock erosion rates at the effective flood exhibit fundamentally different trends depending on whether rock resistance is held constant or allowed to scale with sediment impact energy (Fig. 5a). Under the constant-k_v formulation, bedrock erosion rates at the effective flood decrease systematically with increasing grain size. Although larger grains can detach more material per impact (Fig. 4a), their reduced mobility lowers the impact rate sufficiently to drive an overall decline in erosion rate. Given this, across the explored range of D_{50}, effective-flood erosion rates decrease by nearly an order of magnitude under the assumption of a constant-k_v.

In contrast, when k_v scales inversely with increasing impact energy, instantaneous erosion rates at the effective flood increase with increasing grain size (Fig. 5a). At the coarsest grain sizes, instantaneous bedrock erosion rates plateau, before slightly declining at the coarsest grain sizes because the imposed power-law scaling of k_v limits further gains in erosional efficiency. Importantly, this increase in bedrock erosion rate with increasing grain size at the effective flood is not driven by large differences in bedload impact rate (Fig. 4B). Rather, the impact rate associated with the effective flood varies only slightly between the constant and energy-dependent formulations, exhibiting similar grain-size dependence in both cases. Indeed, the impact rate is slightly lower under the impact-energy-dependent rock resistance formulation across much of the grain-size range. The divergence in bedrock erosion rate at the effective therefore does not arise from increases transport capacity or enhanced particle impact rates. Instead, it reflects changes in detachment efficiency described by the rock

454 resistance coefficient. These results reinforce that incorporating impact-energy-dependent rock
455 resistance fundamentally alters the grain-size sensitivity of effective-flood incision, with
456 differences arising primarily from the scaling of particle mass and detachment efficiency rather
457 than from changes in transport capacity or impact frequency.
458 Across the full range of grain sizes examined, the discharge associated with the effective
459 flood increases monotonically, spanning Q_{eff} ≈ 4–95 m^3/s (Fig. 4b). This systematic increase
460 reflects the greater flow depths required to mobilize coarser grains and achieve transport
461 stages sufficient for abrasion. In dimensional terms, progressively larger floods dominate long-
462 term incision as grain size increases. However, when expressed as dimensionless transport
463 capacity (τ^*/τ_c^*), the effective flood shifts toward lower transport stages with increasing grain
464 size (Fig. 4b). This apparent paradox arises from the nondimensionalization by grain diameter in
465 the Shields formulation (Shields, 1936), where boundary shear stress is normalized by grain
466 size. For a given discharge, increasing D_{50} reduces τ^*, effectively compressing the accessible
467 range of transport stages across the flow distribution. As a result, although larger discharges are
468 required to mobilize coarser sediment, the maximum in frequency-weighted geomorphic work
469 occurs at more moderate τ^*/τ_c^* values because extreme transport stages become increasingly
470 rare. These dynamics are reflected in systematic shifts in the exceedance probability of the
471 effective flood (Fig. 5c). Effective events become progressively less frequent with increasing
472 grain size, declining from ~0.25 at D_{50} = 0.02 m to <0.01 at D_{50}= 0.10 m. This monotonic
473 decrease reinforces the magnitude-frequency tradeoffs between large and small floods, with
474 coarser sediment shifting the effective flood toward larger, rarer floods capable of moving
475 larger particles.
476 This behavior is consistent across both constant- and impact-energy-dependent
477 formulations of rock resistance. Although the energy-dependent case shifts effective work
478 toward higher discharges at a given grain size (Fig. 5b), the differences in Q_{eff} and associated
479 differences in exceedance probabilities remain very small (<10% across all grain sizes). Thus,
480 while individual components of the saltation-abrasion model, specifically the volume removed
481 per unit impact, are strongly influenced by introducing an impact-energy-dependent rock
482 resistance coefficient (Fig. 4), integrating incision across the full flood distribution damps those
483 differences. Weighting incision by flood frequency appears to offset much of the enhanced
484 detachment efficiency at high impact energies, such that the effective flood remains broadly
485 similar between formulations for any given grain size.
486
487 *3.2.2 Contribution of less frequent, high-magnitude floods*
488 To directly evaluate the role of more infrequent, high-magnitude events on total
489 bedrock erosion, we examine how cumulative incision is partitioned across the discharge
490 distribution and how this partitioning changes under impact-energy-dependent rock resistance.
491 Although shifts in effective discharge and its exceedance probability remain small across grain

sizes (Fig. 5), impact energy increases nonlinearly with particle mass and velocity. As a result, larger floods are more likely to have enhanced erosional efficiency under impact-energy-dependent k_v, shifting their overall contribution to cumulative bedrock incision.

We first calculate the cumulative fraction of total incision as a function of discharge for a subset of modeled grain sizes under both constant and impact-energy-dependent rock resistance (Fig. 6a). For all grain sizes and both treatments of rock resistance, cumulative incision increases most rapidly across moderate discharges, reflecting the combined influence of event magnitude and frequency. As grain size increases, the range of discharges that meaningfully contribute to cumulative incision both shifts to larger flows and narrows, reflecting a reduction in the range of flows that can transport sediment and erode bedrock via abrasion. For fine sediment, incision is distributed across a broader range of discharges, and cumulative incision curves decline gradually as progressively larger floods are included in the cumulative fraction calculation. In contrast, coarse sediment restricts abrasion to a much narrower band of high discharges, rendering low-to-moderate flows largely ineffective. Across all grain sizes, incorporating impact-energy-dependent rock resistance shifts a greater fraction of total incision toward the upper tail of the discharge distribution, indicating that a larger portion of total erosion can be attributed to high-magnitude floods. In contrast to the small shifts in the effective flood (Fig. 5), the cumulative distributions reveal a systematic redistribution of incision toward the upper tail of the discharge distribution under impact-energy-dependent rock resistance.

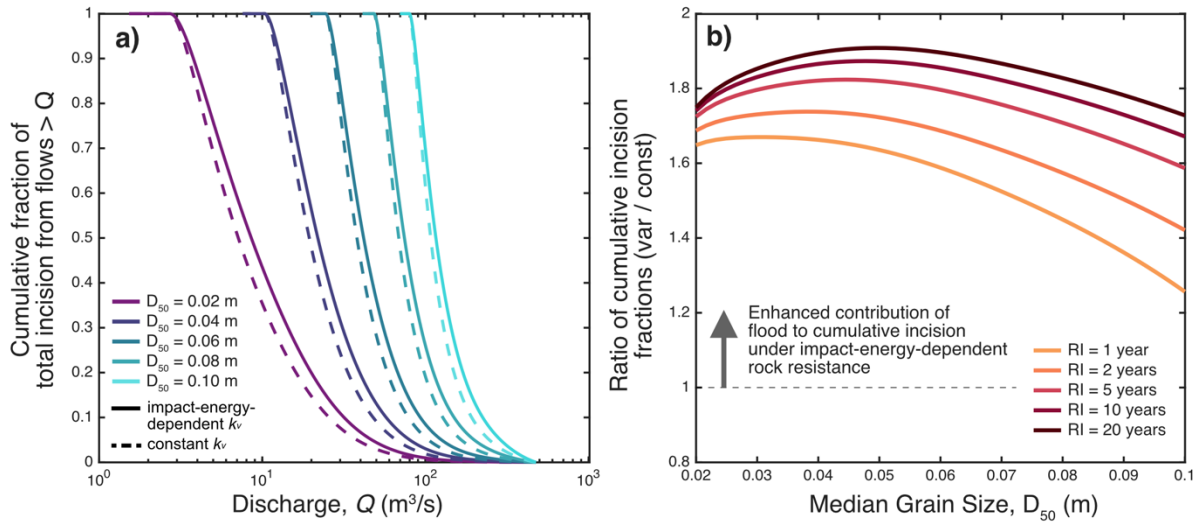

Figure 6. A) Cumulative fraction of total bedrock incision as a function of discharge, *Q*, for a range of grain sizes for impact-energy-dependent rock resistance (black) and constant rock resistance (gray). B) Ratio of cumulative incision predicted by the impact-energy-dependent formulation to that predicted by the constant-resistance case, for a range of recurrence intervals, as a function of grain size.

519

520 This redistribution is more clearly expressed when cumulative incision is explored at
521 specified flood recurrence intervals (Fig. 6b). For recurrence intervals ranging from 1-20 years,
522 we take the ratio of the cumulative fraction of incision of the variable k_v case relative to the
523 constant k_v case. Across all modeled grain sizes, floods with recurrence intervals exceeding 1
524 year contribute more to total incision under impact-energy-dependent rock resistance
525 compared to the assumption of a constant rock resistance, indicating a systematic increase in
526 the relative importance of larger, less frequent floods. It is worth nothing that the magnitude of
527 this increase is not monotonic with sediment caliber. It peaks at intermediate grain sizes, where
528 sediment mobility and impact-energy scaling combine to maximize sensitivity to hydraulic
529 forcing. In this range, floods with 10–20 year recurrence intervals contribute approximately
530 1.8–1.9 times more to total bedrock incision than in the constant-k_v case - an increase of
531 roughly 80–90%. Even more frequent floods with 1–5 year recurrence intervals also show a
532 pronounced contribution to total bedrock incision, exceeding ~60% in this same grain-size
533 window.

534 For finer grains, incision is already distributed across a broad range of discharges, so
535 increasing detachment efficiency at high flows produces a smaller shift in the contribution of
536 high magnitude flows relative to moderate grain sizes. Instead, cumulative erosion remains
537 dominated by smaller, more frequent floods, limiting the relative change in the contribution of
538 rare events. In contrast, for the coarsest grains, incision is already concentrated within high-
539 magnitude floods due to sediment transport constraints. Although impact-energy-dependent
540 rock resistance further increases the incision attributed to these events, the proportional
541 change is smaller than at intermediate grain sizes because the erosion budget is already
542 strongly weighted toward extreme flows. As a result, sensitivity declines at both ends of the
543 grain-size spectrum, producing a pronounced peak in response at intermediate sediment
544 calibers.

545 These results demonstrate that introducing while impact-energy-dependent rock
546 resistance does not substantially alter the effective flood itself, it does redistribute the
547 cumulative incision budget toward less frequent, higher-magnitude events. This redistribution
548 is maximized at intermediate grain sizes where hydraulic forcing and detachment efficiency
549 interact most effectively.

550

551 **4 Discussion**

552 *4.1 Controls on the effective flood under impact-energy-dependent rock resistance*

553 A primary motivation for introducing impact-energy-dependent rock resistance is that
554 particle impact energy increases nonlinearly with both grain size and transport stage (Fig. 2), so
555 erosional efficiency should not be uniform across floods or sediment conditions. Within the
556 saltation-abrasion framework, the effective flood emerges as the discharge that maximizes

frequency-weighted geomorphic work across the flow distribution (Wolman & Miller, 1960; Sklar & Dietrich, 2006). Our results show that allowing k_v to decrease with impact energy fundamentally changes the grain-size sensitivity of the detachment component of the saltation-abrasion model (Fig. 3; 4a). However, these shifts in erosional efficiency per unit impact only slightly shift the effective flood itself for any given grain size (Fig. 4b-c). Importantly, this result reveals that while the physics of individual impacts are strongly altered by incorporation of an impact-energy-dependent rock resistance term, the flood event that maximizes geomorphic work remains anchored by the magnitude-frequency structure of the hydrograph.

The dominant mechanism by which impact-energy-dependent rock resistance affects bedrock incision is through the volume removed per impact, V_{imp}, because k_v enters the detachment expression directly (Sklar & Dietrich, 2004). Under the impact-energy-dependent formulation, V_{imp} at the effective flood spans a much wider dynamic range with grain size than in the constant-k_v case (Fig. 4a), reflecting the combined scaling of impact energy with particle mass and velocity. By contrast, the impact rate I_r and the exposed fraction F_e vary less between variable and constant-k_v formulations (Fig. 4b–c) because they are primarily governed by transport capacity and sediment cover mechanics in SAM rather than by detachment physics (Sklar & Dietrich, 2004; Sklar & Dietrich, 2006).

Despite the strong sensitivity of V_{imp} to impact energy, the effective flood remains broadly similar because the discharge that maximizes long-term incision is determined by the balance between event magnitude and event frequency. Increasing detachment efficiency at high impact energies does not inherently shift dominance to the largest floods, as these events are ultimately de-emphasized by their low exceedance probabilities (Wolman & Miller, 1960; Sklar & Dietrich, 2006). Consequently, the peak in frequency-weighted geomorphic work reflects intermediate-sized flows for both variable and constant-k_v. This behavior is consistent with prior applications of the saltation-abrasion model, which show that incision rates are maximized where transport stage is sufficiently high to generate frequent energetic impacts, yet not so rare that cumulative contribution is limited by infrequent occurrence or by evolving sediment cover dynamics (Sklar & Dietrich, 2006; Sklar & Dietrich, 2008).

Importantly, this partitioning assumes that sediment supply and cover respond deterministically to hydraulics, as prescribed in the canonical SAM framework. In natural channels, however, stochastic sediment inputs from hillslopes, episodic pulses of coarse material, and transient storage can partially decouple F_e from instantaneous hydraulic forcing (DeLisle et al., 2022; DeLisle & Yanites, 2023; Golly et al., 2017; Turowski, 2009). Variability in supply relative to transport capacity can shift the bed between detachment- and transport-limited states, altering both the threshold for erosion and the channel's ability to convey sediment (Finnegan et al., 2007; Johnson, 2016; Johnson & Whipple, 2010). Under conditions of excess supply, persistent or patchy cover may suppress exposure even at high shear stress, limiting the delivery of high-energy impacts. Conversely, sediment-starved conditions may

increase exposure but reduce impact frequency, lowering the cumulative work delivered to the bed. Because impact energy and V_{imp} scale strongly with transport stage, such stochastic modulation of cover and transport efficiency has the potential to reorganize when and how impact energy is transmitted to the bed, potentially shifting erosion thresholds and redistributing geomorphic work across the hydrograph (DeLisle & Yanites, 2023; Turowski, 2009). Thus, while our results isolate the detachment consequences of energy-dependent resistance, natural variability in sediment supply introduces an additional degree of freedom that could amplify or damp the predicted grain-size sensitivity on bedrock incision rates.

4.2 The shifting contribution of less frequent, high-magnitude floods

Notably, our analysis of less frequent, higher-magnitude floods demonstrates that while the effective flood appears to remain relatively constant, this does not imply invariance in the partitioning of overall incision across all flood events. Instead, our recurrence-interval analysis reveals a systematic redistribution of cumulative incision toward the upper tail of the discharge distribution under impact-energy-dependent rock resistance (Fig. 6). This result reinforces that while the effective flood represents a summary of the geomorphic work, identifying the discharge at which frequency-weighted incision is maximized, it does not necessarily describe how incision is distributed across the rest of the discharge distribution. The recurrence-interval incision portioning analysis that we present here, by contrast, integrates incision across portions of the flow distribution and revealing changes in the overall shape of that distribution. Our analysis reveals that under impact-energy-dependent resistance, a greater fraction of total incision is accomplished by less frequent, higher-magnitude events.

This behavior parallels results from variable-discharge stream-power models in which erosion thresholds determine which portions of the hydrograph contribute to long-term incision (Tucker & Bras, 2000; Snyder et al., 2003; Lague et al., 2005; DiBiase & Whipple, 2011). In those frameworks, increasing the incision threshold may not shift the discharge that maximizes geomorphic work, yet it alters the relative contribution of the distribution tails by concentrating incision into flows that exceed that threshold. Here, impact-energy-dependent resistance operates through a different mechanism, enhancing the efficiency of bedrock detachment rather than directly modifying entrainment threshold, but produces a similar outcome by increasing the erosive effectiveness of high-energy impacts during larger floods.

These findings have broader implications for landscape-scale modeling. First, they provide a process-based pathway for explicitly incorporating bedload impact energy, and by extension, sediment-transport driven differences in bedrock detachment efficiency, into models of long-term incision. In SPIM-like formulations, thresholds are often implemented phenomenologically by introducing a critical shear stress or modifying erodibility without explicitly specifying what sets this threshold or how it evolves with sediment transport conditions. In contrast, the saltation–abrasion framework defines the relevant erosion threshold mechanistically as the boundary shear stress required to mobilize sediment, and ties

incision directly to sediment entrainment, impact delivery, and bed cover. Incorporation of an impact-energy-dependent resistance extends this framework by demomnstrating that even when the entrainment threshold is fixed, the efficiency of impacts above this threshold can vary strongly with grain size and discharge. In this treatment, bedrock erodibility becomes an emergent property of coupling hydraulics and sediment transport.

Importantly, because the erosion threshold is explicitly linked to sediment mobilization, this framework also allows variability in grain-scale motion thresholds to be incorporated directly into long-term incision models. Critical Shields stress is known to vary with channel slope(Lamb et al., 2008; Prancevic & Lamb, 2015), flood magnitude and intermittency (Masteller et al., 2019; Masteller et al., 2025; Ockelford et al., 2019), reworking of riverbed structure (Hodge et al., 2013; Masteller & Finnegan, 2017; Ockelford & Haynes, 2013; Whitfield et al., 2025), and shifts in sediment supply (Hassan et al., 2020; Johnson, 2016; Yager et al., 2012), all of which influence sediment mobility. These process-driven variations in mobility thresholds influence both the frequency and intensity of particle impacts during floods of a given size. By explicitly coupling these threshold dynamics to impact-energy-dependent resistance, the saltation–abrasion framework provides a mechanistic route for linking hydrologic variability, sediment caliber, and bedrock erosion efficiency across the full flood distribution.

Our results reinforce that the effective flood alone is not sufficient to capture the relative contribution of rare, large magnitude flows on overall bedrock incision rates. We find that the effective discharge only shifts slightly between constant and impact-energy-dependent formulations of rock resistance. However, exploration of low-recurrence interval floods reveals a redistribution of cumulative incision toward rarer floods, particularly at intermediate grain sizes. The effective flood metric obscures this shift because it does not capture changes in the skewness or tail weighting of incision across the hydrograph. This distinction is critical for interpreting landscape response to hydroclimatic shifts that disproportionately alter the tails of flood distributions. Even if the nominal effective discharge remains stable, increases in flood intermittency or intensity may elevate the geomorphic influence of rare events. Likewise, shifts in sediment caliber or mobility may also alter the sensitivity of bedrock incision to extreme flows. These results highlight the need for long-term incision models to further explore both grain-scale erosion thresholds and impact-energy-dependent shifts in erosional efficiency, and to account for how these processes redistribute geomorphic work across the full flood distribution.

5 Conclusions and future work

In this contribution, we introduced an impact-energy-dependent rock resistance coefficient into the saltation-abrasion model, which calculates bedrock erosion rates as a function of sediment transport rates. We found that incorporating this variable rock resistance

alters bedrock incision predictions primarily by changing efficiency of bedrock detachment per unit impact at the grain scale. Under this formulation, rock resistance decreases as impact energies increase, amplifying the grain-size dependence of the volume removed per impact. At a constant-discharge experiments, this produces a strong reduction in rock resistance with increasing grain size and a corresponding systematic increase in the volume of material detached per impact relative to a constant resistance assumption.

When the full discharge distribution is considered, these component-level shifts translate into two reach-scale outcomes. First, the effective flood remains broadly similar for a given grain size, indicating that the discharge that maximizes frequency-weighted geomorphic work is still largely set by magnitude-frequency tradeoffs within the discharge distribution. Second, despite minimal changes in the effective flood, the cumulative incision budget shifts toward less frequent, higher-magnitude events under impact-energy-dependent rock resistance, increasing the relative contribution of the upper tail of the flood distribution. This effect is maximized for intermediate grain sizes where impacts become substantially more energetic while sediment remains sufficiently mobile to sustain abrasion.

Two limitations are worth emphasizing when interpreting these results into long-term models for bedrock incision or in field application. First, the impact-energy-dependent scaling of the rock resistance coefficient, is experimentally constrained but derived using surrogate materials and a specific impactor configuration, and then rescaled to span a range reflecting natural rocks (Auel et al., 2017b; Turowski et al., 2013; Masteller et al., 2024). While the relative trends are mechanistically-motivated, extending the framework across lithologies and transport-driven distributions in impact trajectories will require additional calibration and testing. Second, the modeling isolates grain size while holding channel geometry and slope fixed to attribute differences in incision partitioning to the mechanics of bedrock detachment. In natural channels, changes in sediment caliber and discharge regime have strong feedbacks with channel width, slope, and bed state, which in turn alter transport stage, cover, and the reach's capacity to translate impacts into incision (Finnegan et al., 2017; Gasparini et al., 2007; Yanites, 2018) (Gasparini et al., 2007; Yanites, 2018). Incorporating these feedbacks is a natural next step for assessing how impact-energy-dependent resistance influences long-profile form and transient channel adjustment.

Motviated by these results, future experimental work should aim to better constrain the relationship between particle impact energy and rock resistance across representative natural lithologies, sediment shapes, and mixed-size populations. Flume experiments should also quantify how impact angle, impactor material, and bed condition alter the fraction of kinetic energy transmitted to fracture growth. To better characterize the consequences of these impact-energy-dependent differences in rock resistance on channel form, modeling should could explore how channel width, slope, and bed cover to evolve with variable sediment supply and discharge regime. By coupling grain-scale processes with evolution of channel form, this

work could evaluate whether the observed redistribution of incision toward rarer floods has an extractable signature on equilibrium channel morphology.

Acknowledgments

Open Research

All code developed as part of this study is available in a Zenodo repository (Masteller, 2026). *Note to editors and reviewers: The Zenodo repository is currently accessible as a draft with the sharing link below, however, the data are not yet formally published with a DOI. The formally published data will be cited here and linked with a DOI following review. This delay is to enable edits to the dataset if substantive methodological changes are suggested during the review process resulting in material changes to the data.*

https://zenodo.org/records/18851708?preview=1&token=eyJhbGciOiJIUzUxMiJ9.eyJpZCI6IjdhNzViNzY0LWM0MWQtNGNlOS1iOGUwLTg0ZTVkYzQyNzg1ZCIsImRhdGEiOnt9LCJyYW5kb20iOiIzYjRkYzE3ZDE5ZGM2Y2IxZTUxM2M5NjZmZDVjNjY4YiJ9.CLBZ4WzEV5f5cKVLoA1QLN3NS1Q-LvmZjhOGlPVFC7W0IbHiIqJi3skbcvo0PSSlgjcpUnBhSbY0pMGeKj0Bfw

Conflict of Interest Disclosure

The authors declare there are no conflicts of interest for this manuscript.

References

Auel, C., Albayrak, I., Sumi, T., & Boes, R. M. (2017a). Sediment transport in high-speed flows over a fixed bed: 1. Particle dynamics: Sediment transport in high-speed flows: 1. Particle dynamics. *Earth Surface Processes and Landforms*, *42*(9), 1365–1383. https://doi.org/10.1002/esp.4128

Auel, C., Albayrak, I., Sumi, T., & Boes, R. M. (2017b). Sediment transport in high-speed flows over a fixed bed: 2. Particle impacts and abrasion prediction: Sediment transport in high-speed flows: 2. Particle impacts. *Earth Surface Processes and Landforms*, *42*(9), 1384–1396. https://doi.org/10.1002/esp.4132

DeLisle, C., & Yanites, B. J. (2023). Rethinking Variability in Bedrock Rivers: Sensitivity of Hillslope Sediment Supply to Precipitation Events Modulates Bedrock Incision During Floods. *Journal of Geophysical Research: Earth Surface*, *128*(9), e2023JF007148. https://doi.org/10.1029/2023JF007148

DeLisle, C., Yanites, B. J., Chen, C.-Y., Shyu, J. B. H., & Rittenour, T. M. (2022). Extreme event-driven sediment aggradation and erosional buffering along a tectonic gradient in southern Taiwan. *Geology*, *50*(1), 16–20. https://doi.org/10.1130/G49304.1

DiBiase, R. A., & Whipple, K. X. (2011). *The influence of erosion thresholds and runoff variability on the relationships among topography, climate, and erosion rate*. Journal of Geophysical Research, 116(F4), F04036.

748 Duvall, A., Kirby, E., & Burbank, D. (2004). Tectonic and lithologic controls on bedrock channel
749 profiles and processes in coastal California. *Journal of Geophysical Research: Earth*
750 *Surface*, *109*(F3). https://doi.org/10.1029/2003JF000086
751 Ferrier, K. L., Huppert, K. L., & Perron, J. T. (2013). Climatic control of bedrock river incision.
752 *Nature*, *496*(7444), 206–209. https://doi.org/10.1038/nature11982
753 Ferrier, K. L., Perron, J. T., Mukhopadhyay, S., Rosener, M., Stock, J. D., Huppert, K. L., &
754 Slosberg, M. (2013). Covariation of climate and long-term erosion rates across a steep
755 rainfall gradient on the Hawaiian island of Kaua'i. *GSA Bulletin*, *125*(7–8), 1146–1163.
756 https://doi.org/10.1130/B30726.1
757 Finnegan, N. J., Sklar, L. S., & Fuller, T. K. (2007). Interplay of sediment supply, river incision, and
758 channel morphology revealed by the transient evolution of an experimental bedrock
759 channel. *Journal of Geophysical Research*, *112*(F3), F03S11.
760 https://doi.org/10.1029/2006JF000569
761 Finnegan, N. J., Schumer, R., & Finnegan, S. (2014). A signature of transience in bedrock river
762 incision rates over timescales of 104–107 years. *Nature*, *505*(7483), 391–394.
763 https://doi.org/10.1038/nature12913
764 Finnegan, N. J., Klier, R. A., Johnstone, S., Pfeiffer, A. M., & Johnson, K. (2017). Field evidence
765 for the control of grain size and sediment supply on steady-state bedrock river channel
766 slopes in a tectonically active setting. *Earth Surface Processes and Landforms*, *42*(14),
767 2338–2349. https://doi.org/10.1002/esp.4187
768 Forte, A. M., Leonard, J. S., Rossi, M. W., Whipple, K. X., Heimsath, A. M., Sukhishvili, L., et al.
769 (2022). Low variability runoff inhibits coupling of climate, tectonics, and topography in
770 the Greater Caucasus. *Earth and Planetary Science Letters*, *584*, 117525.
771 https://doi.org/10.1016/j.epsl.2022.117525
772 Gasparini, N. M., Whipple, K. X., & Bras, R. L. (2007). Predictions of steady state and transient
773 landscape morphology using sediment-flux-dependent river incision models. *Journal of*
774 *Geophysical Research: Earth Surface*, *112*(F3). https://doi.org/10.1029/2006JF000567
775 Golly, A., Turowski, J. M., Badoux, A., & Hovius, N. (2017). Controls and feedbacks in the
776 coupling of mountain channels and hillslopes. *Geology*, *45*(4).
777 Han, J., Gasparini, N. M., Johnson, J. P. L., & Murphy, B. P. (2014). Modeling the influence of
778 rainfall gradients on discharge, bedrock erodibility, and river profile evolution, with
779 application to the Big Island, Hawai'i. *Journal of Geophysical Research: Earth Surface*,
780 *119*(6), 1418–1440. https://doi.org/10.1002/2013JF002961
781 Hancock, G. S., Small, E. E., & Wobus, C. (2011). Modeling the effects of weathering on bedrock-
782 floored channel geometry. *Journal of Geophysical Research: Earth Surface*, *116*(F3).
783 https://doi.org/10.1029/2010JF001908
784 Hartshorn, K. (2002). Climate-Driven Bedrock Incision in an Active Mountain Belt. *Science*,
785 *297*(5589), 2036–2038. https://doi.org/10.1126/science.1075078

786 Hassan, M. A., Saletti, M., Johnson, J. P. L., Ferrer-Boix, C., Venditti, J. G., & Church, M. (2020).
787 Experimental Insights Into the Threshold of Motion in Alluvial Channels: Sediment
788 Supply and Streambed State. *Journal of Geophysical Research: Earth Surface*, *125*(12),
789 e2020JF005736. https://doi.org/10.1029/2020JF005736
790 Hodge, R. A., Sear, D. A., & Leyland, J. (2013). Spatial variations in surface sediment structure in
791 riffle-pool sequences: a preliminary test of the Differential Sediment Entrainment
792 Hypothesis (DSEH): Spatial Variations in Sediment Structure in Riffle-Pool Sequences.
793 *Earth Surface Processes and Landforms*, *38*(5), 449–465.
794 https://doi.org/10.1002/esp.3290
795 Howard, A. D. (1994). A detachment-limited model of drainage basin evolution. *Water*
796 *Resources Research*, *30*(7), 2261–2285. https://doi.org/10.1029/94WR00757
797 HOWARD, A. D., & KERBY, G. (1983). Channel changes in badlands. *GSA Bulletin*, *94*(6), 739–
798 752. https://doi.org/10.1130/0016-7606(1983)94%253C739:CCIB%253E2.0.CO;2
799 Johnson, J. P. L. (2016). Gravel threshold of motion: a state function of sediment transport
800 disequilibrium? *Earth Surface Dynamics*, *4*(3), 685–703. https://doi.org/10.5194/esurf-4-
801 685-2016
802 Johnson, J. P. L., & Whipple, K. X. (2010). Evaluating the controls of shear stress, sediment
803 supply, alluvial cover, and channel morphology on experimental bedrock incision rate.
804 *Journal of Geophysical Research: Earth Surface*, *115*(F2), 2009JF001335.
805 https://doi.org/10.1029/2009JF001335
806 Johnson, J. P. L., Whipple, K. X., Sklar, L. S., & Hanks, T. C. (2009). Transport slopes, sediment
807 cover, and bedrock channel incision in the Henry Mountains, Utah. *Journal of*
808 *Geophysical Research*, *114*(F2), F02014. https://doi.org/10.1029/2007JF000862
809 Kirby, E., & Whipple, K. X. (2012). Expression of active tectonics in erosional landscapes. *Journal*
810 *of Structural Geology*, *44*, 54–75. https://doi.org/10.1016/j.jsg.2012.07.009
811 Lague, D., Davy, P., & Crave, A. (2000). Estimating uplift rate and erodibility from the area-slope
812 relationship: Examples from Brittany (France) and numerical modelling. *Physics and*
813 *Chemistry of the Earth, Part A: Solid Earth and Geodesy*, *25*(6–7), 543–548.
814 Lague, D., Hovius, N., & Davy, P. (2005). *Discharge, discharge variability, and the bedrock*
815 *channel profile*. Journal of Geophysical Research: Earth Surface, 110(F4).
816 Lamb, M. P., Dietrich, W. E., & Venditti, J. G. (2008). *Is the critical Shields stress for incipient*
817 *sediment motion dependent on channel-bed slope? Journal of Geophysical Research,*
818 *113(F2)*.
819 Larimer, J. E., Yager, E. M., Yanites, B. J., & Witsil, A. J. C. (2021). Flume Experiments on the
820 Erosive Energy of Bed Load Impacts on Rough and Planar Beds. *Journal of Geophysical*
821 *Research: Earth Surface*, *126*(4), e2020JF005834. https://doi.org/10.1029/2020JF005834
822 Leonard, J. S., & Whipple, K. X. (2021). Influence of Spatial Rainfall Gradients on River
823 Longitudinal Profiles and the Topographic Expression of Spatially and Temporally

Variable Climates in Mountain Landscapes. *Journal of Geophysical Research: Earth Surface*, *126*(12), e2021JF006183. https://doi.org/10.1029/2021JF006183

Litwin Miller, K., & Jerolmack, D. (2021). Controls on the rates and products of particle attrition by bed-load collisions. *Earth Surface Dynamics*, *9*(4), 755–770. https://doi.org/10.5194/esurf-9-755-2021

Masteller, C. C., & Finnegan, N. J. (2017). Interplay between grain protrusion and sediment entrainment in an experimental flume. *Journal of Geophysical Research: Earth Surface*, *122*(1).

Masteller, C. C., Finnegan, N. J., Turowski, J. M., Yager, E. M., & Rickenmann, D. (2019). History-Dependent Threshold for Motion Revealed by Continuous Bedload Transport Measurements in a Steep Mountain Stream. *Geophysical Research Letters*, *46*(5).

Masteller, C. C., Chandler, H., & Bower, J. (2024). The Fluvial Battering Ram: Collisional Experiments Reveal the Importance of Particle Impact Energies on Bedrock Erosional Efficiency. *Geophysical Research Letters*, *51*(14), e2024GL109533. https://doi.org/10.1029/2024GL109533

Masteller, Claire C., Johnson, J. P. L., Rickenmann, D., & Turowski, J. M. (2025). Modeling memory in gravel-bed rivers: a flow-history-dependent relation for evolving thresholds of motion. *Earth Surface Dynamics*, *13*(4), 593–605. https://doi.org/10.5194/esurf-13-593-2025

Masteller, C.C., Philips, C.B., Kostynick, R.P., Castejon-Villalobos, J.F., Lopez, C.G., Shallue, M.K., Bower, J., Sigman, A., Tracking the trajectory of alluvial channel adjustment along a river's profile: under review at Geophysical Research Letters.

Mitchell, N. A., & Yanites, B. J. (2021). Bedrock river erosion through dipping layered rocks: quantifying erodibility through kinematic wave speed. *Earth Surface Dynamics*, *9*(4), 723–753. https://doi.org/10.5194/esurf-9-723-2021

Ockelford, A., Woodcock, S., & Haynes, H. (2019). The impact of inter-flood duration on non-cohesive sediment bed stability. *Earth Surface Processes and Landforms*, *44*(14).

Ockelford, A.-M., & Haynes, H. (2013). The impact of stress history on bed structure. *Earth Surface Processes and Landforms*, *38*(7).

Prancevic, J. P., & Lamb, M. P. (2015). Unraveling bed slope from relative roughness in initial sediment motion: Relative roughness and incipient motion. *Journal of Geophysical Research: Earth Surface*, *120*(3), 474–489. https://doi.org/10.1002/2014JF003323

Scherler, D., DiBiase, R. A., Fisher, G. B., & Avouac, J.-P. (2017). Testing monsoonal controls on bedrock river incision in the Himalaya and Eastern Tibet with a stochastic-threshold stream power model. *Journal of Geophysical Research: Earth Surface*, *122*(7), 1389–1429.

Seidl, M., & Dietrich, W. E. (n.d.). The Problem of Channel Erosion into Bedrock. *CATENA SUPPLEMENT*.

Shields, A. (2021). *Application of similarity principles and turbulence research to bed-load movement*. Retrieved January 13.

Sklar, L., & Dietrich, W. (2008). Implications of the saltation–abrasion bedrock incision model for steady-state river longitudinal profile relief and concavity. *Earth Surface Processes and Landforms*, *33*, 1129–1151. https://doi.org/10.1002/esp.1689

Sklar, L. S., & Dietrich, W. E. (2004). A mechanistic model for river incision into bedrock by saltating bed load. *Water Resources Research*, *40*(6). https://doi.org/10.1029/2003WR002496

Sklar, L. S., & Dietrich, W. E. (2006). The role of sediment in controlling steady-state bedrock channel slope: Implications of the saltation–abrasion incision model. *Geomorphology*, *82*(1–2), 58–83. https://doi.org/10.1016/j.geomorph.2005.08.019

Small, E. E., Blom, T., Hancock, G. S., Hynek, B. M., & Wobus, C. W. (2015). Variability of rock erodibility in bedrock-floored stream channels based on abrasion mill experiments: ROCK ERODIBILITY IN BEDROCK CHANNELS. *Journal of Geophysical Research: Earth Surface*, *120*(8), 1455–1469. https://doi.org/10.1002/2015JF003506

Snyder, N. P., Whipple, K. X., Tucker, G. E., & Merritts, D. J. (2003). Importance of a stochastic distribution of floods and erosion thresholds in the bedrock river incision problem. *Journal of Geophysical Research: Solid Earth*, *108*(B2).

Tucker, G. E., & Bras, R. L. (2000). A stochastic approach to modeling the role of rainfall variability in drainage basin evolution. *Water Resources Research*, *36*(7), 1953–1964. https://doi.org/10.1029/2000WR900065

Tucker, G. E., & Slingerland, R. L. (1994). Erosional dynamics, flexural isostasy, and long-lived escarpments: A numerical modeling study. *Journal of Geophysical Research: Solid Earth*, *99*(B6), 12229–12243. https://doi.org/10.1029/94JB00320

Turowski, J. M. (2009). Stochastic modeling of the cover effect and bedrock erosion. *Water Resources Research*, *45*(3). https://doi.org/10.1029/2008WR007262

Turowski, J. M., Böckli, M., Rickenmann, D., & Beer, A. R. (2013). Field measurements of the energy delivered to the channel bed by moving bed load and links to bedrock erosion: ENERGY DELIVERED BY MOVING BED LOAD. *Journal of Geophysical Research: Earth Surface*, *118*(4), 2438–2450. https://doi.org/10.1002/2013JF002765

Whitfield, D., Baynes, E. R. C., Hodge, R. A., Rice, S. P., & Yager, E. M. (2025). The Influence of Gravel-Bed Structure on Grain Mobility Thresholds: Comparison of Force-Balance Approaches. *Journal of Geophysical Research: Earth Surface*, *130*(5), e2025JF008333. https://doi.org/10.1029/2025JF008333

Willgoose, G., Bras, R. L., & Rodriguez-Iturbe, I. (1991). A physical explanation of an observed link area-slope relationship. *Water Resources Research*, *27*(7), 1697–1702. https://doi.org/10.1029/91WR00937

Wobus, C., Whipple, K. X., Kirby, E., Snyder, N., Johnson, J., Spyropolou, K., et al. (2006). Tectonics from topography: Procedures, promise, and pitfalls. In S. D. Willett, N. Hovius, M. T. Brandon, & D. M. Fisher (Eds.), *Tectonics, Climate, and Landscape Evolution* (Vol. 398, p. 0). Geological Society of America. https://doi.org/10.1130/2006.2398(04)

Wolman, M. G., & Miller, J. P. (1960). Magnitude and Frequency of Forces in Geomorphic Processes. *The Journal of Geology*, *68*(1), 54–74.

Yager, E. M., Turowski, J. M., Rickenmann, D., & McArdell, B. W. (2012). Sediment supply, grain protrusion, and bedload transport in mountain streams. *Geophysical Research Letters*, *39*(10).

Yanites, B. J. (2018). The Dynamics of Channel Slope, Width, and Sediment in Actively Eroding Bedrock River Systems. *Journal of Geophysical Research: Earth Surface*, *123*(7), 1504–1527. https://doi.org/10.1029/2017JF004405

PUBLICATIONS

Journal of Geophysical Research – Earth Surface

Supporting Information for

Implications of impact-energy dependent erosional efficiency on bedrock river sediment dynamics and form: 1. Reach-scale dynamics and the effective flood

Claire C. Masteller[1]

1 Department of Earth, Environmental, and Planetary Sciences, Washington University in St. Louis, Saint Louis, MO 63130

Contents of this file

Introduction

- This supplementary file contains one table defining the model parameter values used in this study and their values (Table S1). It also contains one figure, Figure S1, demonstrating the distribution of impact kinetic energies for the constant discharge case explored in the main manuscript.

940

941 **Table S1.**

942 List of model parameter values for reference field site, reference values from Sklar and Dietrich,
943 2006.

944

Parameter name	Parameter symbol	Units	Value
Drainage area	A	km^2	112
Slope	S	m/m	0.005
Discharge-drainage area coefficient	c		0.347
Discharge-drainage area exponent	h		1
Channel width	w	m	18
Depth-discharge scaling coefficient	k		0.3147
Depth-discharge scaling exponent	f		0.4321
acceleration due to gravity	g	m/s^2	9.81
Density of water	ρ	kg/m^3	1000
density of sediment	ρ_s	km/m^3	2650
Submerged sediment density	R_b		1.65
Dynamic viscosity	μ	Pa s	0.00
critical Shields stress	τ_c^*		0.03
Rock tensile strength	σ_T	Pa	7000000.00
Young's modulus	Y	Pa	50000000000.00
Sediment supply rate	Q_s	kg/s	42.60
Median rock resistance coefficient	k_v		19880.00
Minimum rock resistance coefficient	$k_{v\,min}$		1000.00
Maximum rock resistance coefficient	$k_{v\,max}$		10000000.00
Median grain size, reference site	D_{50}	m	0.06

945

946

947

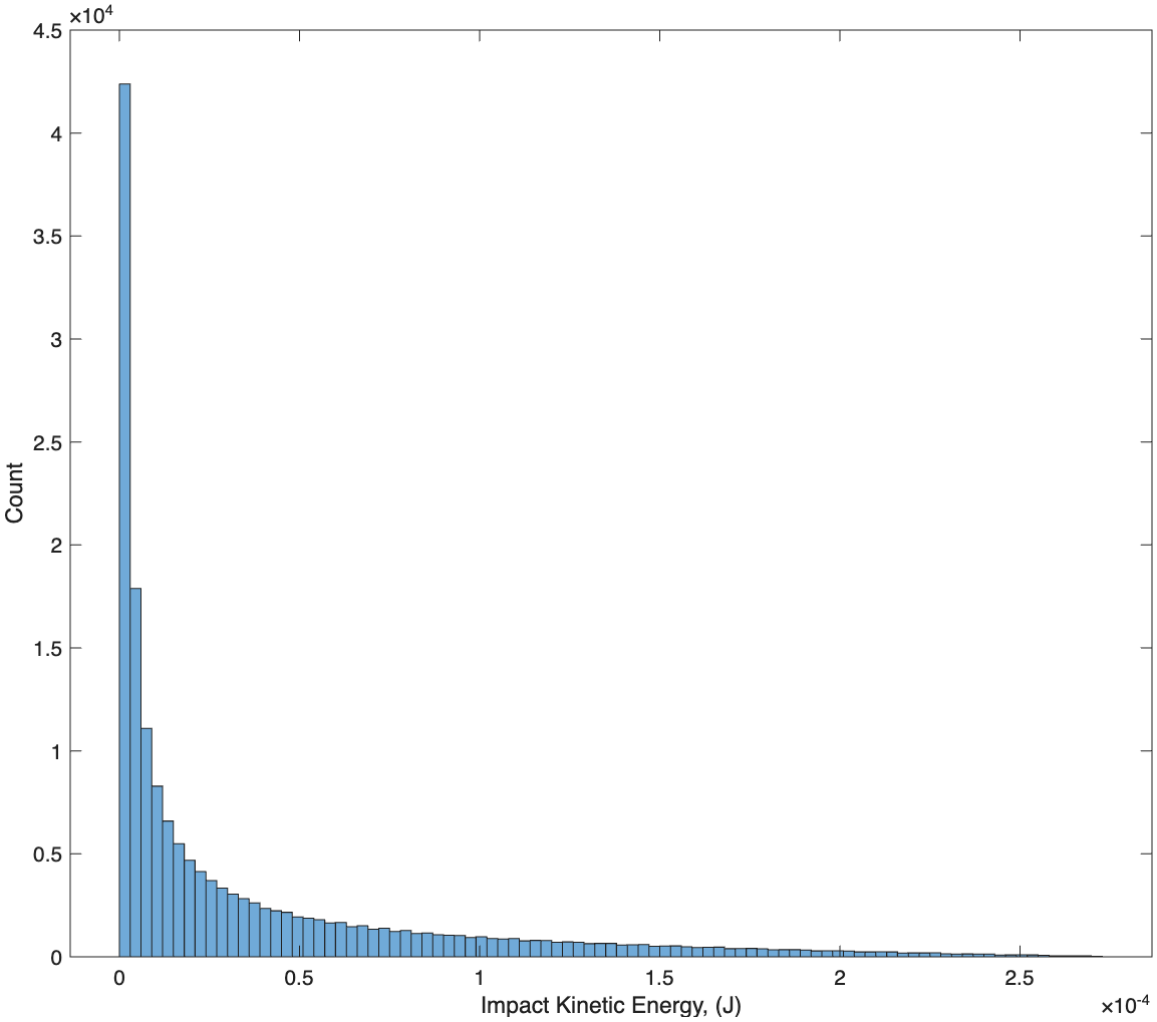

948

949 **Figure S1.** Distribution of Impact Kinetic Energy, KE_{imp} (J), for the constant discharge case

950

951

952

953